The Finite Element Modeling of the Resistance Spot Welding Process

An analytical tool is provided to predict the processing parameters needed to produce a spot weld with sufficient joint penetration

BY H. A. NIED

ABSTRACT. Resistance spot welding is a complicated process, which involves the interaction of electrical, thermal, mechanical, and metallurgical phenomena. An axisymmetric finite element model to simulate this coupled process was developed, using isoparametric solid elements to represent the electrode and workpiece, and boundary elements to represent surface contact conditions.

The model was used for analyzing the squeeze and weld cycles to determine the electrical, thermal, and mechanical responses. Predictions of the temperature distribution, thermal expansion and associated stresses, and weld nugget geometry were obtained from this model. Extensive resistance spot welding tests were conducted on Type 321 stainless steel sheets to validate the finite element model. Comparison of the analytic results to test data are presented and discussed.

Introduction

Resistance spot welding was invented in 1877 by Elihu Thomson and has been widely used since then as a manufacturing process for joining sheet metal. Even though resistance spot welding is over 100 years old, the physics of the process has not been well understood; however, this has not hindered its industrial application for joining a large variety of metals.

Paper presented at the 64th Annual AWS Convention held in Philadelphia, Pennsylvania, during April 24-29, 1983.

H. A. NIED is a Staff Mechanical Engineer, Process Technology Branch, Corporation Research and Development, General Electric Company, Schenectady, New York.

Some Fundamentals

The electrical resistance spot welding process for joining two materials at their common interface is a complicated interaction of electrical, thermal, mechanical, metallurgical, and surface phenomena. Figure 1 is a simplified representation of the process, showing some of the essential features for producing a weld. A brief description of this welding process is warranted, since it will help identify features that should be included in a theoretical model to provide a realistic simulation.

The water-cooled copper electrodes provide essentially three functions:

1. Their low electric resistance provides a conduit to carry high current to the workpiece without significant Joule heating losses.
2. Their high thermal conductivity provides a method to control the nugget formation and cool-down by conducting heat from the workpiece.
3. The electrodes exert a concentrated force on the outer surfaces of the materials to be joined.

The electrode force produces a local deformation at the common interface to seat the workpiece properly and to establish good electrical contact before current flow. It should be noted that this initial load generates high contact stresses between the electrodes and workpiece. Repeated mechanical cycling can contribute to the mechanical fatigue and distortion of the electrode.

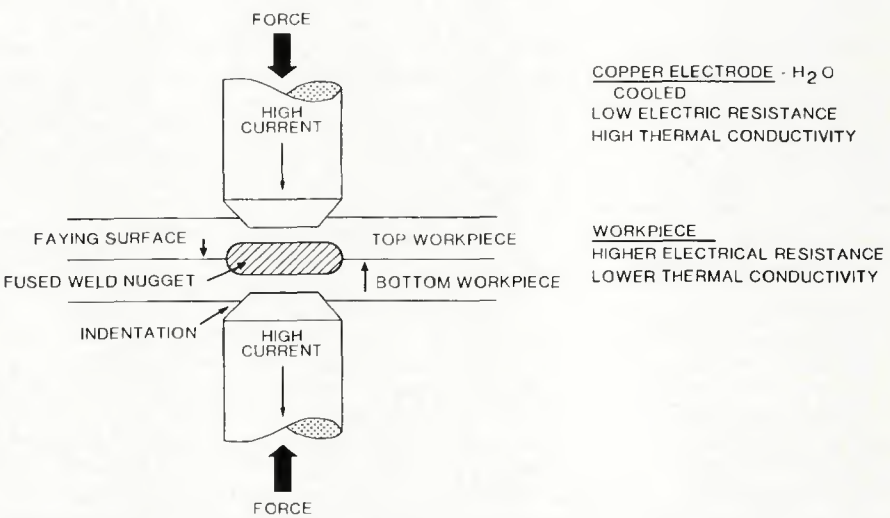

Fig. 1—Resistance spot welding process

The total electrical resistance of the system consists of the bulk material resistances of the copper electrodes and workpieces plus the surface contact resistance at each material interface. These interface resistances are due to surface films, oxides, and asperities. A high electrode force, which produces a localized compressive interface stress, will mechanically break down these surface conditions, thereby providing good interfacial electrical and thermal conductance.

Since the resistance of the copper electrodes and metals to be joined is small, a large current flow is needed to produce a high Joule heating effect in the workpiece. The largest voltage drop occurs in the workpiece, since the specific resistivity of the copper electrodes is an order of magnitude lower than the metals to be joined. This generates the highest internal heat production in the workpiece, thereby producing a temperature distribution in both the workpiece and electrodes. The transient heating generates thermal expansion and stresses due to the high temperature gradients.

If the high current is maintained for a sufficient length of time, melting will initiate at the common interface of the workpieces and spread to produce the weld nugget. This phase change from solid to liquid produces a drastic change in material properties. During the weld cycle, the electrode load is maintained to offset the high internal thermal expansion and, thereby, contain the molten metal within the workpiece. This prevents liquid metal expulsion.

It is obvious that, during the welding cycle, the electrode load also helps to maintain proper electrical and thermal contact until the formation of the weld nugget is completed. The weld cycle is terminated by switching the current off while maintaining the electrode load. The final stage of the process is the hold cycle, which establishes the metallurgical quality of the weld nugget. During the hold cycle, the nugget cools and contracts. Mechanical load is essential to provide the necessary forging pressure to obtain a good metallurgical structure and to prevent the formation of shrinkage voids. The hold time is also important, since it establishes the rate of cooling as long as electrode contact is maintained.

Early Mathematical Modeling

Since the physics of the process is so complicated, it is quite understandable that very little was published in the open literature on the mathematical modeling which covers these many aspects. A survey of the literature on this subject shows that the mathematical and experimental analyses were chiefly directed to surface phenomena or heat transfer modeling. However, there is published information (Refs. 1 and 2) concerning both experimental and theoretical investigations of electric current flow in conducting solids. These two references are considered fundamental for a better understanding of the resistance spot welding process.

Bowen and Williamson (Ref. 1) have shown that the interface between two solids in contact possesses a constriction resistance due to surface asperities. The response of the contact region to pulses of current was studied, and it was shown that the temperature in the contact region could be calculated, based on the potential difference across the constriction. Bowen and Williamson's observations revealed that the temperature at the interface between two solids under constant load produced a softening of the metal locally which increased the contact area.

Greenwood and Williamson (Ref. 2) formulated a theoretical model to determine the spatial distribution of the current and the associated temperature distribution between two semi-infinite solids in contact over a small area. Their analysis showed that current density singularities occurred at the periphery of contact. Experiments were conducted on two sheets of steel using ordinary welding equipment. The results revealed that the production of heat was greatest near the periphery of contact where the melting point was reached before the center. Clearly, any mathematical model of the resistance spot welding process should be able to predict this singularity phenomenon in the early stages of the welding cycle.

Most of the theoretical modeling described in the open literature has been directed to predicting the temperature distribution during welding without including the thermomechanical response. Greenwood (Ref. 3) was the first to develop a heat conduction model to simulate the resistance spot welding process. He formulated a linear, axisymmetric heat transfer model of the process which included the internal heat production due to current flow. The model did not include the geometry of the electrode but simulated its influence by an effective boundary condition. It assumed the local heat flux at the electrode/workpiece interface was equal to the thermal conductivity of the electrode times the temperature difference between the workpiece and coolant.

Numerical results were obtained using a finite difference method to solve the partial differential equation for temperature-independent thermal properties. The spatial temperature distributions were obtained over time ranges representative of the welding process. The results revealed that temperature concentrations occurred at the periphery of the electrode/workpiece interface early in the weld cycle. This mechanism was predicted and observed by Greenwood previously (Ref. 2). Temperature distributions were also obtained at longer times, showing the characteristic isotherms of an elliptic-shaped weld nugget. In this formulation, Greenwood did not include the latent heat of fusion associated with phase change. The theoretical model is significant in its contribution, since it exhibits all the major features of the electrothermal characteristics of the process.

Bentley and Greenwood (Ref. 4) conducted experiments to study the temperature distribution at different stages during the formation of spot welds in mild steel. Comparisons between theory and experiment were conducted over a range of typical weld cycle times for low carbon steel. Their results showed that the theory provided a good indication of actual temperature distribution in the later stages of weld nugget formation. During the early times of welding, the contact resistance at the sheet to sheet interface played a dominant role in the heat production. However, this contact resistance decreased rapidly to a minimum in the first few half cycles of the welding process; consequently, Greenwood's model, which does not include surface resistance, did not provide temperature distributions in agreement with the experiments at the early stage of welding. This is not considered to be a detrimental limitation to the model as a predictive tool.

Modeling in the 1960's and 1970's

Publications of theoretical modeling of the resistance spot welding process in the decade 1967-1977 were sparse. Three papers (Refs. 5-7) reveal that the analyses in that period were chiefly devoted to determining temperature distributions. Rice (Ref. 5) developed a one-dimensional multilayer model of the resistance spot welding process which included bulk Joule heating, interfacial surface resistance, and temperature-dependent electrical and thermal properties. This model did not include the latent heat of fusion due to phase change. Chakalev (Ref. 6) formulated an axisymmetric heat transfer model of spot welding similar to Greenwood's model and also used the finite difference method to solve the heat conduction equation. Latent heat of fusion was included in the numerical analysis. The method used to include latent heat was not made clear in that paper.

Houchens (Ref. 7) developed two theoretical heat transfer models to study the resistance spot welding process. The first model was a one-dimensional heat transfer model which included the temperature-dependent material properties of

both the workpiece and electrode. The latent heat effect was included in that model by using the fictitious specific heat increase at the temperature between solidus and liquidus. The second model was an axisymmetric electrothermal simulation of the resistance spot welding process, which included the geometry of a flat-end electrode in contact with the workpiece.

Solutions to both formulations were obtained by using the finite difference technique. The one-dimensional model required a nonlinear analysis since the current density and heat conduction equations were coupled through the temperature. The solution to the axisymmetric model required a solution of the current density and heat conduction equation independently since they became uncoupled when the assumption of temperature independent properties was invoked. Houchens (Ref. 7) reported that the one-dimensional process model provided insight into the dynamics of weld nugget penetration, while the axisymmetric model provided information on current density and temperature distribution in both the workpiece and electrode.

In all the publications cited, the analytical models of the resistance spot welding process were focused on the heat transfer response, while the thermomechanical coupling was completely neglected. These analyses required assuming the contact area at the outset. Consequently, the contact area between the electrode and workpiece was reasonably assumed as equal to the diameter of the flat on the end of the electrode. However, the contact diameter at the faying surface is unknown and load-dependent. Since the contact area established during the squeeze cycle is dependent on the electrode load used, it is obvious that an initial assumption of the contact diameter can be a source of large error, especially if spherical-end electrodes are used in the process.

It is the purpose of this present work to include the nonlinear thermomechanical coupling and contact behavior into a theoretical model to provide a more realistic simulation of the welding process. Consequently, a single finite element model of the welding process was developed to include the electro-thermal mechanical coupling.

Finite Element Modeling

The finite element method of analysis is essentially the numerical solution of the governing field or partial differential equations by the discretization of the continuum. According to this method, the original geometry is replaced by an array of elements consisting of nodes in the interior and on the surface of the material. The model response is sought for a single element such that the continuity of the function is preserved between the nodes while satisfying the governing field equations in the interior. For example, the finite element formulation for an elasticity problem can be derived by using the principle of virtual work for determining nodal displacements such that compatibility is satisfied exactly and equilibrium approximately in the interior. Once the nodal response of a single element has been derived, the global behavior of the solid is then obtained by summing up the contribution for each individual element. Accordingly, this formulation reduces the original problem to the solution of coupled simultaneous equations, which can be compactly written in matrix notation.

One of the chief features of the finite element technique is the way curved boundaries can be realistically treated by using higher order isoparametric elements. Accurate solutions can be obtained in regions where the gradients are steep by refining the mesh. It can be shown that as the nodal degrees of freedom are increased by refining the mesh, the solution will generally converge to the exact solution of the governing equation.

The finite element method of analysis has been recognized as a powerful tool and has been effectively used to obtain solutions in solid mechanics, heat transfer, and fluid dynamics. The theory of finite elements and their applications are contained in many references too numerous to list; however, the work authored by Bathe and Wilson (Ref. 8) is a good source which explains much of the theory used.

Model Development

An axisymmetric finite element model was developed to simulate the spot welding process during the sequential stages of squeeze, weld, and hold cycles. For the case of equal thickness workpieces and equal electrode geometry, only one quadrant of the model has to be constructed due to geometric symmetry about the centerline of the electrodes and the common interface between the workpieces. This simplification of the model which reduces the number of elements and computing costs is shown in cross section in Fig. 2.

The types of finite elements used and the boundary conditions are shown in Fig. 3. Isoparametric solid quadratic finite elements were used to represent the electrode and workpiece. Surface elements were included in the model to account for surface effects such as electrical resistance, thermal conductivity, and local deformation at the interfaces between the electrode/workpiece and the faying surface between the workpieces to be joined. These surface elements are represented as springs merely for convenience of illustration and should not be considered as a spring element.

The length of the surface element (usually of nearly zero thickness) can be chosen approximately equal to surface oxide thicknesses. This surface element simulates three types of surface conditions. For simulating surface mechanical deformation (Hertzian contact), it has the property to transfer compressive stress, but will not support tensile load. This feature is important to determine the contact area which generally varies with electrode load. In addition, this element will allow relative slip between the electrode and workpiece due to the difference in their thermal expansion. For electrothermal surface conditions, it can be used to simulate the electrical surface resistance and thermal conductance associated with surface oxides and films.

The boundary conditions imposed on the finite element model are also shown in Fig. 3. The mechanical load was applied as a pressure distribution on the annular end of the electrode as shown. This load could have been made time-dependent during the analysis, but was held constant. The electrical boundary condition was imposed as a potential drop

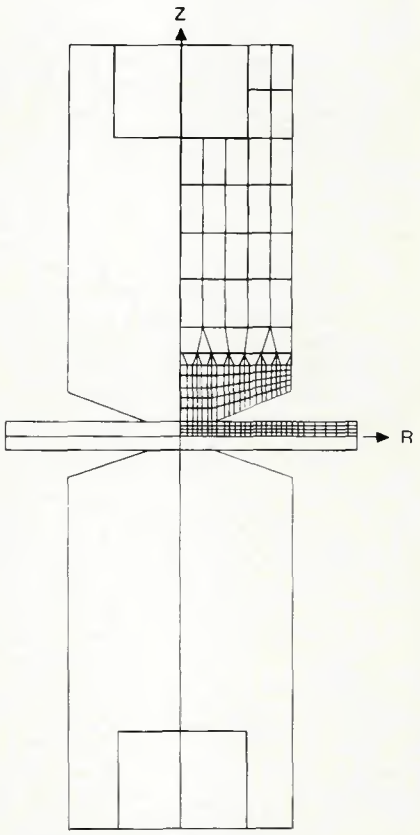

Fig. 2 – Resistance spot welding axisymmetric model showing application of symmetry

between the end of the electrode and the interface between the workpieces. Convective heat transfer conditions are imposed in the water-cooling cavity by the specification of a heat transfer coefficient representative of the flow rate used in the test welding unit. Convective heat transfer to ambient air was specified on all the lateral surfaces of the electrode and workpiece not in contact. All of the lateral surfaces of the workpiece except the surfaces in contact were specified as stress-free. Symmetry boundary conditions for radial displacement and thermal and potential gradients were specified as zero on the centerline along the Z axis. At the interface between the workpieces to be joined, the temperature gradient and electric potential were set equal to zero over the contact region; while in the gap between sheets separated under load, the current and normal stress was set equal to zero.

Cycle Simulation

At the beginning of the squeeze cycle, the initial conditions of stress and electric potential are set equal to zero, while the temperature is specified as room temperature. Just prior to the application of the load, flat contact at the surface between the workpieces is assumed. After the electrode load application, the electrode indentation and the contact established at the faying surface becomes the geometric boundary conditions for the welding cycle. The initial conditions for the welding cycle are now the deformation and state of stress established during the squeeze cycle, while the temperature remains constant at ambient and the electric potential is zero.

The welding phase is simulated by assuming a step increase in potential applied to the electrode for a time period equivalent to the number of weld cycles. This electric potential is essentially equivalent to the root-mean-square (RMS) value of a sinusoidal applied voltage. It should be noted that any time-varying potential could have been applied to this model, though for this investigation an equivalent RMS value was considered as a reasonable applied potential. During the welding phase, the transient temperatures, current density, thermal expansion, and state of stress change rapidly. These responses can be determined successively for each weld cycle.

The hold phase is analyzed by a step decrease in potential drop to zero. The removal of the applied voltage terminates the current flow. However, the temperature and stress state attained up to the end of the welding phase become the initial conditions for the transient cool-down analysis.

Role of Material Properties

Isotropic temperature-dependent material properties were used for both the electrothermal and structural analysis. These properties were specified over a temperature range from room temperature to above melting. The material properties used in the molten state were extrapolated from various sources.

The electrothermal analysis required specifying the following material properties: thermal conductivity, electrical resistivity, density, specific heat, and melting temperature. In addition, the thermal stress analysis required using elastic mod-

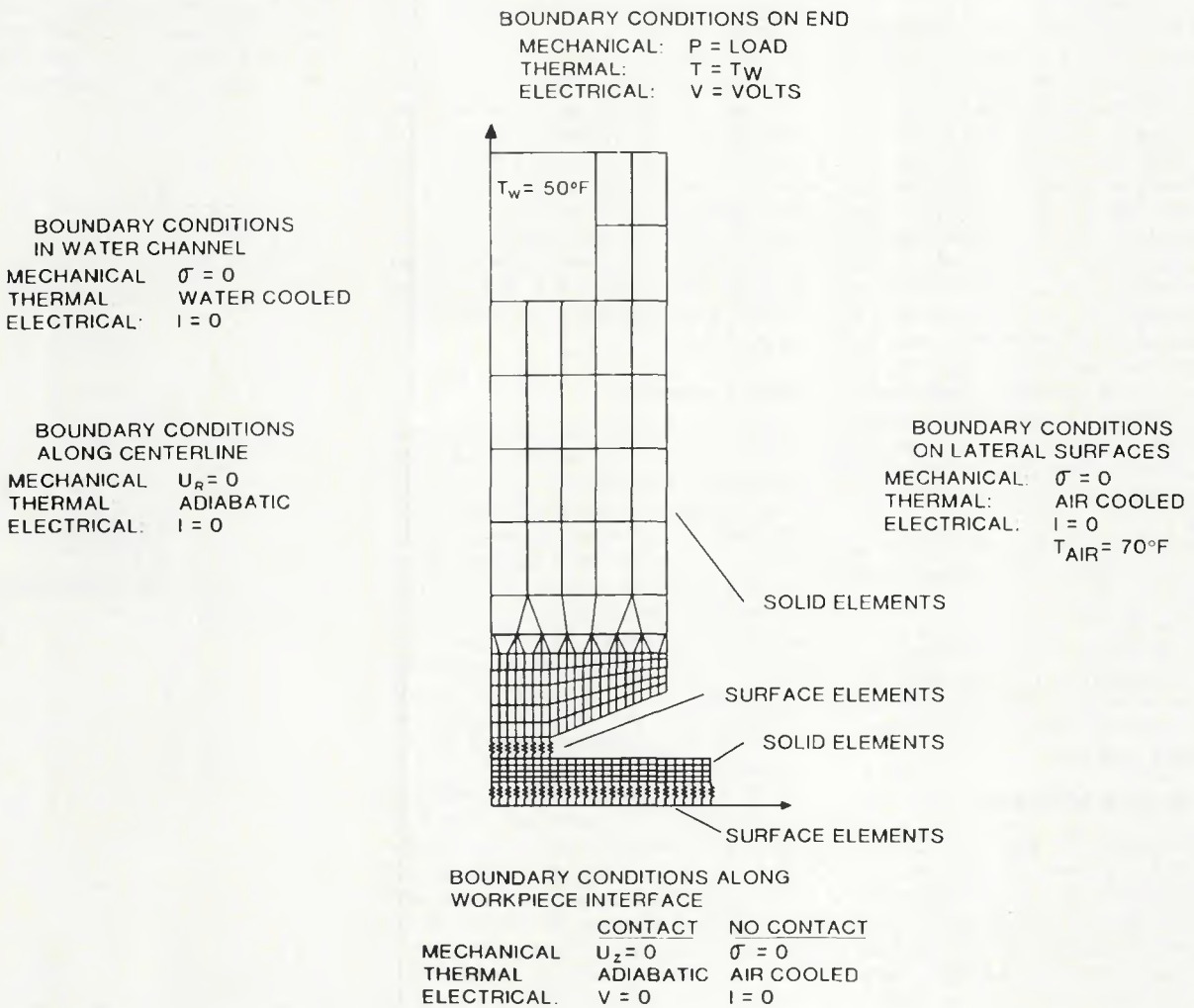

Fig. 3—Identification of finite element types and boundary conditions

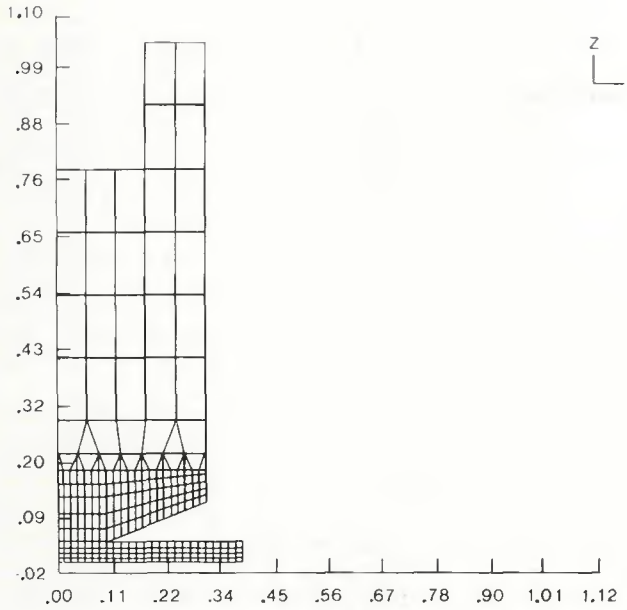

Fig. 4—Finite element geometry of electrode and workpiece

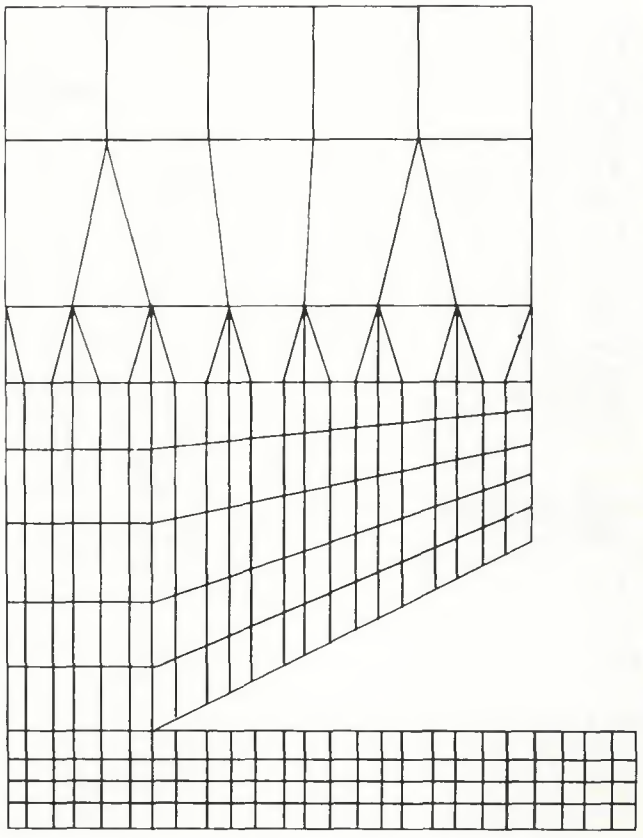

Fig. 5 (right)—Enlarged view of model at end of electrode

ulus, Poisson's ratio, and coefficient of expansion. The latent heat of fusion was included in the analysis once the melting temperature was attained by using the fictitious specific heat method. Erickson (Ref. 9) compared the various numerical methods for including the heat of fusion in a phase change problem. The method used was found to give satisfactory results for many transient heat transfer calculations.

Model Features and Capabilities

The finite element model just described can be constructed from standard finite element computer codes having extensive element libraries which are on the market. Some of these general purpose computer codes have added flexibility, which enable one to add elements for special coupling applications. In this investigation, the ANSYS finite element program was used to construct the model and to conduct the analyses.

The geometry of the finite element model used for the analyses is shown in Figs. 4 and 5. Figure 4 shows the mesh for the entire geometry of the electrode and workpiece which consisted of 311 elements and 356 nodes.

Only a 1 in. (25.4 mm) section at the end of the electrode, which is normally 3 in. (76.2 mm) long, was modeled. The shank diameter of this electrode was equal to ⅝ in. (16.0 mm) with an end face diameter of 0.18 in. (4.6 mm). The workpiece geometry was 0.040 in. (1 mm) thick with a 1 in. (25.4 mm) diameter.

Closeup details of the finite element mesh are shown in Fig. 5. The mesh size at the end of the electrode was found to be sufficiently refined for the determination of the variables and their gradients in the region of interest. Since the temperature and stress gradients on the upper section of the electrode were small, a coarse mesh could be used without sacrificing solution accuracy.

The finite element model of the resistance spot welding process includes the following features and capabilities:

Geometry.

1. Three electrode configurations.
   - Flat-end electrode.
   - Tapered-end electrode.
   - Spherical-end electrode.
2. Electrode internal water cooling channel.
3. Variable thickness workpiece.

Input.

1. Electrode mechanical force.
2. Applied voltage/current.
3. Welding time.

Heat Transfer Boundary Conditions.

1. Internal water cooling.
2. External convective heat transfer to air.

Surface Conditions.

1. Mechanical contact condition between electrode/workpiece interface and workpiece surfaces.
2. Electrical and thermal contact conditions between electrode/workpiece interface and workpiece surfaces.

Temperature-Dependent Material Properties for Electrode and Workpiece.

1. Thermal conductivity.
2. Resistivity.
3. Specific heat.
4. Density.
5. Young's modulus.
6. Coefficient of expansion.
7. Poisson's ratio.
8. Melt temperature.

Finite Element Output/Results.

1. Radius of electrical contact between electrode/workpiece interface and workpiece surfaces.
2. Radius of thermal contact between electrode/workpiece interface and workpiece surfaces.
3. Indentation of electrode into workpiece.
4. Voltage drop distribution in workpiece.
5. Temperature distribution in electrode and workpiece during weld cycle.
6. Melt front interface in workpiece.
   - Shape of weld nugget.
   - Weld nugget penetration.
   - Weld nugget expansion.
7. Deformation of electrode and workpiece during welding cycle.
8. Thermal stress distribution in elec-

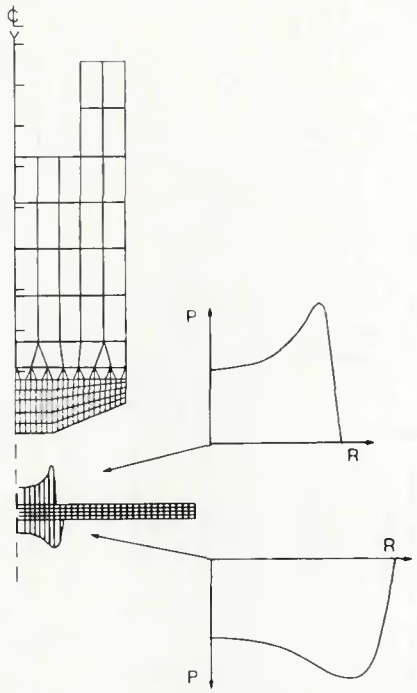

Fig. 6—Characteristic contact pressure distributions for a truncated electrode setup

trode and workpiece during weld cycle.

9. Prediction of expulsion and 'stuck' weld conditions.

Results and Discussion

Finite element analyses of the resistance spot welding process were conducted for two types of electrode configurations: truncated and spherical-end electrodes. Due to space limitations, only the results of the analysis for the truncated electrode are described here. In addition, although the model has the capability to analyze the entire process from squeeze to cooldown, only the squeeze and welding phases are presented, since they are vital for the determination of the weld nugget geometry.

The analysis was conducted using Class III copper and Type 321 austenitic stainless steel material properties for the electrode and workpiece, respectively.

Squeeze Cycle Analysis

It has been previously pointed out that one of the most important features of the finite element model is that the areas of contact between the electrode and workpiece and at the faying surface, which are unknowns in the problem, can be determined. All the models previously published to simulate spot welding assume the size of the interface contacts at the outset of their analysis.

For this investigation, a squeeze cycle analysis was conducted to determine the contact areas including the associated pressure distribution and local deformation when a mechanical load of 1000 lb (4448 N) was applied. Figure 6 depicts the characteristic pressure distribution at the contact regions when a truncated electrode is used for the process. Figure 7 compares the pressure distributions at the two contact surfaces. At the interface between the electrode and workpiece, a maximum contact stress of 38 ksi (262 MPa) is attained near the edge of the flat on the truncated electrode. This contact stress profile shows that the compressive stress at the center is less than the annular region near the corner of the electrode.

If the electrode had been assumed to be a rigid (nondeformable) material, a stress singularity would have been obtained in the workpiece at the edge of the electrode. Similarly, the contact pressure between the workpieces has the same characteristic profile, *i.e.*, the stress is higher near the edge of contact than at the center. At that interface, a maximum contact stress of 33 ksi (227.5 MPa), which is less than at the electrode/workpiece interface, is generated. The contact diameter is larger at the faying surface than between the electrode and workpiece. The contact diameter at the faying surface was found to be 0.24 in. (6.1 mm) in diameter, while at the electrode interface it was 0.18 in. (4.6 mm). The diameter of contact between the electrode and workpiece is essentially equal to the face diameter of the electrode, since the indentation was small.

Figure 8 shows the local deformation that occurs in the electrode and workpiece. The electrode indents the workpiece 4.48×10^{-3} in. (1.14×10^{-2} mm), which is slight. In Fig. 8, the dashed lines show the original geometry before the load is applied. The concentrated contact pressure exerted on the workpiece causes the workpiece to lift up in the area beyond the common contact interface between the workpieces. Furthermore, Fig. 8 indicates that there is relative slip between the electrode and workpiece shown by the offset in the node points. This surface response under mechanical loading could not have been obtained without the use of surface elements.

For the analysis, the coefficient of friction was assumed to be equal to zero. Results obtained by the finite element method showing high edge stresses at the edge of an electrode and workpiece separation are in agreement with results obtained by Civelek (Ref. 10) using an integral equation formulation. The results of the squeeze analysis have revealed that not only are the contact stresses nonuniform, but that the state of strain produced by the electrode load produces a separation of the workpieces beyond the radius of contact.

These effects are easily demonstrated by experiment. Furthermore, the analysis has shown that a truncated electrode has a unique pinching action in an annular

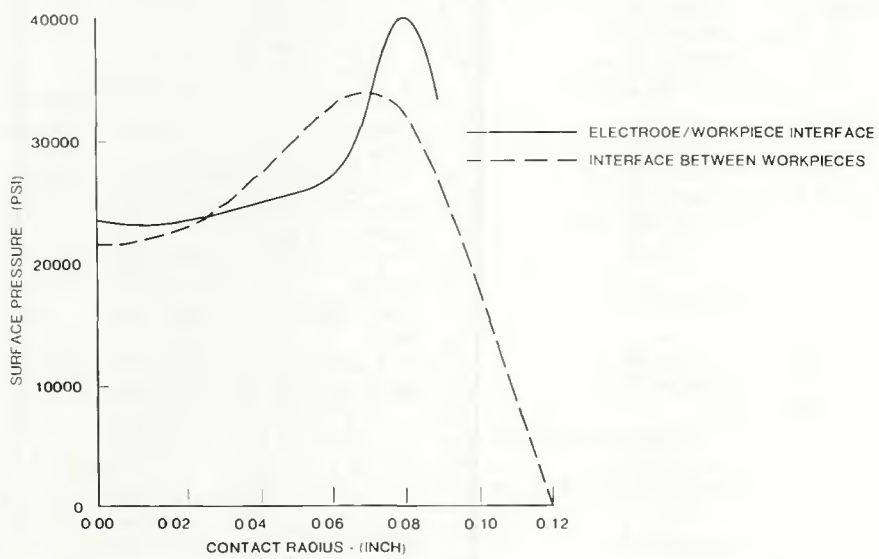

Fig. 7—Comparison of contact pressure distributions at the two contact surfaces

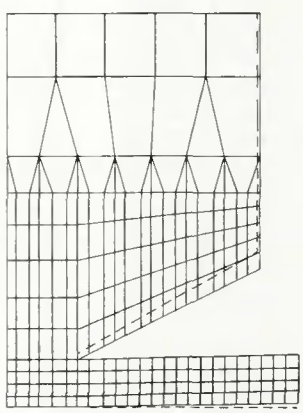

Fig. 8—Finite element model mesh deformation due to 1000 lb (4448 N) electrode load

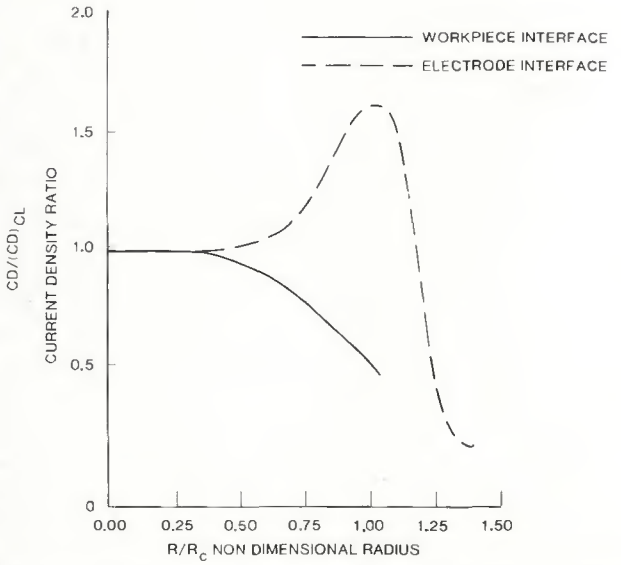

Fig. 9—Current density ratio vs. non-dimensional radius; time = 2 cycles

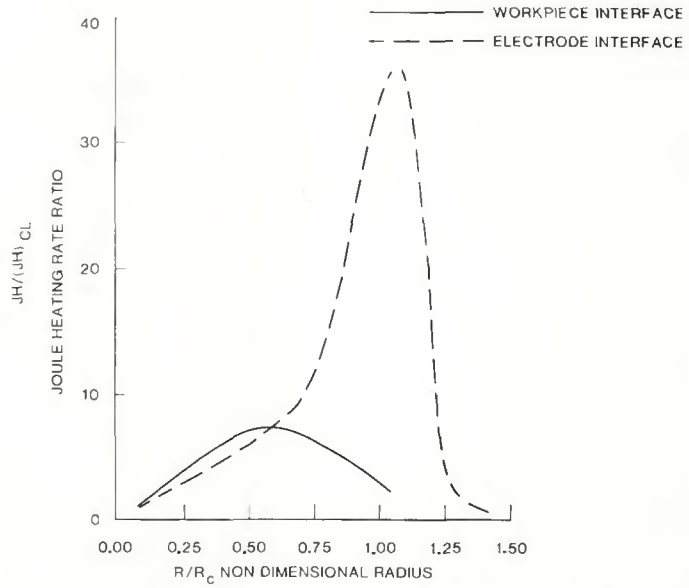

Fig. 10—Joule heating rate ratio vs. non-dimensional radius; time = 2 cycles

region at the interface between the workpieces; this is desirable to prevent liquid metal expulsion during welding. However, the high contact stress at the edge of the electrode will eventually lead to permanent deformation in that vicinity during cyclic loading.

Weld Cycle Analysis

The weld cycle analysis was conducted by imposing a potential drop of 0.45 V on the finite element model between the top surface of the electrode and the contact surface at the workpiece interface. This potential drop is equivalent to a total voltage drop of 0.9 V applied across the electrodes, which was determined by experiment.

The ambient air temperature was specified as 70°F (21.1°C). The water cooling temperature was set equal to 50°F (10°C). The electrode load of 1000 lb (4448 N) set during the squeeze analysis was maintained constant during the welding process. Welding time was varied from two cycles (⅓₀ s) to ten cycles (⅙ s) to determine the transient temperature distributions, thermal expansion, and thermal stresses generated in both the electrode and workpiece.

At a welding time of two cycles, melting was not predicted to occur. Figure 9 compares the current density profile along the electrode/workpiece interface to the faying surface interface at this time. The ordinate is the current density ratio relative to the value at the centerline. The abscissa is the radius ratio relative to the radius of contact. A maximum in the current density distribution occurs near the periphery of contact between the electrode and workpiece. The current density distribution along the faying surface is a maximum at the center and diminishes with increasing radius.

Figure 10 compares the Joule heating rates at the two surfaces. The Joule heating rate ratio is plotted relative to the magnitude at the center line. The highest heat production occurs at a location near the edge of the electrode, while the heating rate is an order of magnitude less along the faying surface. This phenomenon of high heat production in the vicinity of the electrode edge early in the welding phase was first noted by Greenwood (Ref. 2, 3, 4) in discussing the results of his analysis. His experiments validated that response.

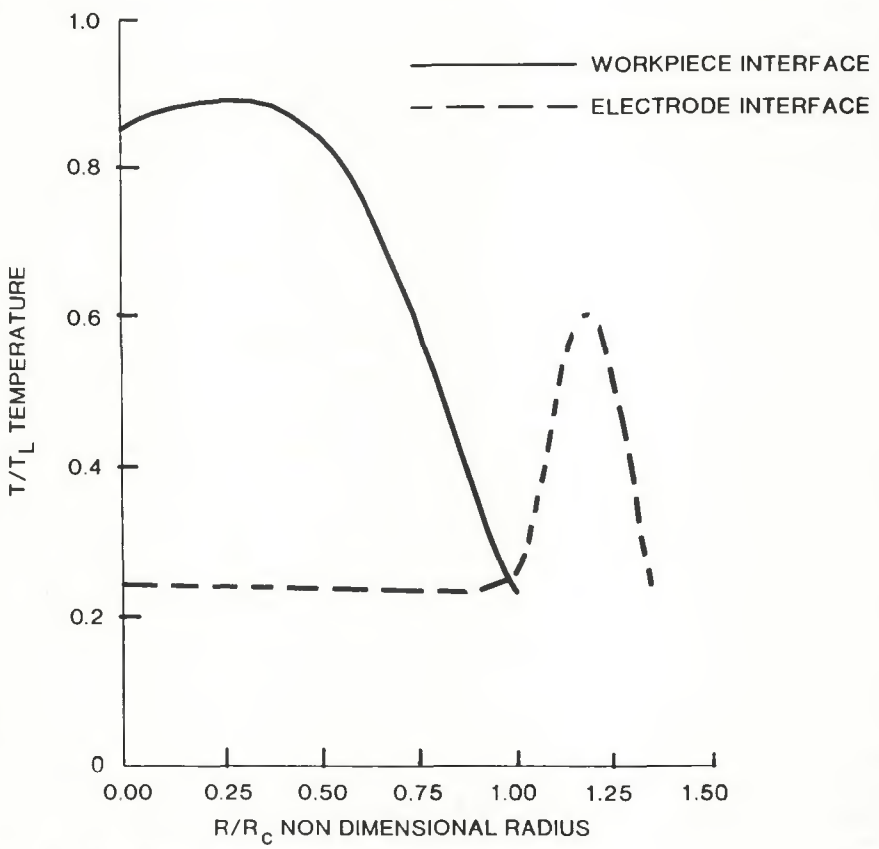

Fig. 11—Temperature ratio vs. non-dimensional radius; time = 2 cycles

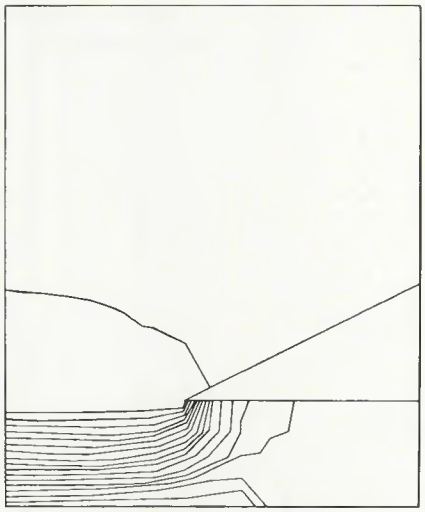

Fig. 12 – Equipotential distribution; time = 7 cycles

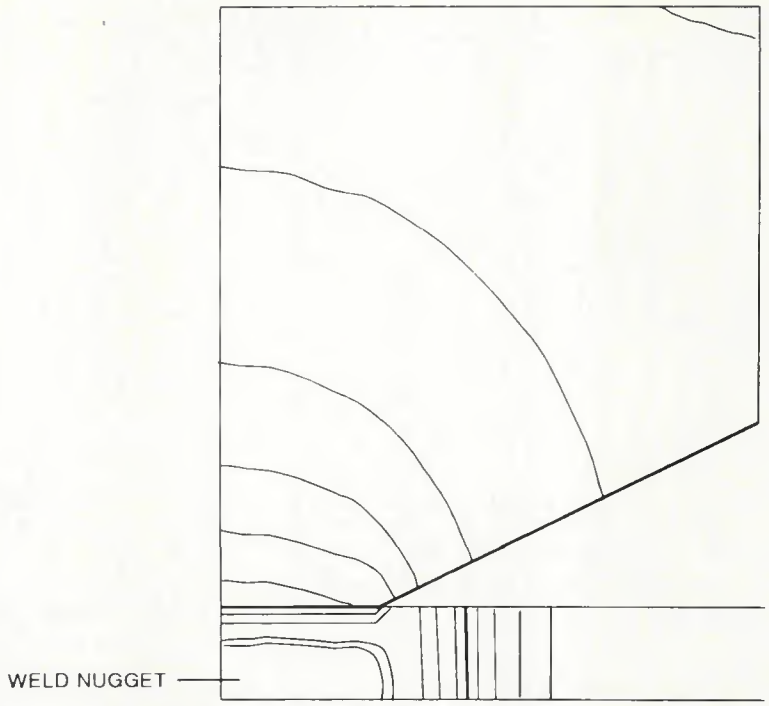

Fig. 13 – Weld nugget geometry and isotherm distribution; time = 7 cycles

Figure 11 compares the temperature distribution at the two contact surfaces for the weld time at two cycles. The temperature ratio is taken with respect to the liquidus temperature equal to 2600°F (1427°C). The temperature along the faying surfaces reduces as the radius approaches the outer edge of contact. The temperature distribution at the electrode/workpiece interface is less than in the interior due to the heat conduction into the electrode. However, there is a temperature maximum along this surface in an annular region beyond the edge of the electrode.

Satoh *et al.* (Ref. 11) provide a good experimental benchmark for the temperature distribution in a cross-sectional plane through the weld nugget. The authors developed a temperature distribution measurement method which uses a two dimensional specimen to simulate spot welding at the early stages. Their technique of using a surface temperature indicator (coating) in conjunction with high-speed photography was used to determine the influences of electrode force and shape, breakdown of oxide layer, and effect of contact resistance. The temperature distributions obtained using the finite element model agreed with the trends and temperature distributions reported in that reference.

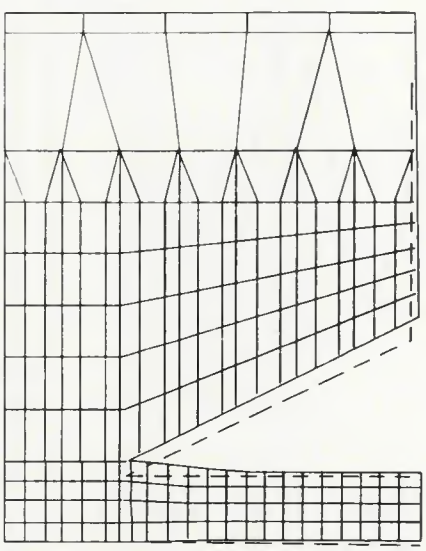

Fig. 14 – Thermal expansion of electrode and workpiece; time = 7 cycles

Analysis conducted with increasing time revealed that melting first occurred along the workpiece faying surface at 2.5 cycles. The point of melting does not occur on the center line of the specimen but is slightly offset. This is not a discrepancy in the model or analysis. It is a physical response to internal heat production in a material which is temperature-dependent. The weld nugget essentially forms as a toroid about the centerline. This molten zone expands rapidly to fill in the center region of the toroid in the next few cycles until a penny-shaped nugget is formed. During the weld nugget formation, growth rate is not equal in the thickness and radial directions. As the nugget approaches the electrode/workpiece interface, the penetration rate decreases and the radial growth rate increases.

By the end of the seventh welding cycle, a weld nugget geometry has been formed; it has 65% penetration and a nugget diameter equal to 0.180–0.188 in. (4.57–4.78 mm). The analytic results obtained at this welding time are shown in Figs. 12 through 15. The lines of equipotential set up by the impressed voltage are shown in Fig. 12. The greatest potential drop occurs through the workpiece thickness, which shows the greatest line density. A total current of 8046 A flows through the workpiece.

Figure 13 shows the weld nugget surrounded by the isotherms which are generated by the Joule heating effect. These isotherms are superimposed in the original geometry of the electrode and workpiece. The weld nugget geometry can be clearly seen.

The two isotherms which form the envelope of the weld nugget are the solidus and liquidus isotherms, respectively. For Type 321 stainless steel, the solidus and liquidus temperatures are 2500°F (1371°C) and 2600°F (1427°C), respectively. The weld nugget height and diameter were determined as 0.052 in. (1.32 mm) and 0.180 in. (4.57 mm), respectively.

Figure 14 shows the accumulated thermal expansion, which has occurred by the end of the seventh cycle. The view shows the local deformation in the workpiece and the electrode. The dashed lines show the original geometry, and the solid lines show the expanded state. The relative slip at the electrode/workpiece interface due to differential expansion is small. Most of the thermal expansion occurs directly under the electrode due to the large thermal expansion created by the phase change in the weld nugget.

A total thermal expansion between the electrodes for the full model shown in

Fig. 2 was predicted to be 0.00564 in. (0.143 mm). This value of expansion is double the value obtained from one quadrant of the model. The expansion value is cited in this form, since experimental values of nugget expansion are measured by the relative displacement of the upper electrode to the lower electrode, which is fixed.

Figure 15 shows the vertical stress distribution in the electrode and workpiece. Note that the combined thermal and mechanical load produce a compressive state of stress in the vertical direction. Due to the thermal expansion, the largest contact pressure occurs along the center line. This distribution is different from the contact stresses determined for the squeeze cycle.

Experiments

Tests were conducted in the laboratory using a 150 kVA, single-phase Taylor-Winfield spot welding machine which operated at 440 V, 60 cycle power. The maximum short-circuit secondary current was 38,000 A. The electrodes and machine were instrumented for spot welding tests conducted on Type 321 pickled stainless steel specimens 0.04 in. (1.02 mm) thick, 0.625 in. (15.875 mm) wide, and 4 in. (10.16 cm) long. The electrodes were instrumented with voltage probes, thermocouples, and an accelerometer for the upper electrode only. The current was measured using a calibrated Duffers current meter. A digital optical encoder was used to measure the relative thermal expansion between the electrodes.

Experiments were conducted for different electrode loads, current, and welding times to obtain data for validating the finite element model. The welding machine settings are made on the welding unit controls by setting the weld time cycles for squeeze, weld, and hold. The current setting is made on the percent heat control.

Comparisons of experimental results and finite element model predictions are shown in Figs. 16 and 17 for a welding current of 8000 A. Figure 16 is a plot of the weld nugget expansion as a function of welding time in cycles where the solid and dotted lines represent the model and experimental data, respectively. At a time of two cycles or below, melting has not occurred. After three to four cycles, stuck welds which lack joint penetration are produced. At a time of ten cycles and above, weld expulsion will occur.

The finite element model gave good agreement with the experimental results. The specimens which were welded were sectioned with a diamond wheel. The cross-section was polished and etched. The weld nugget joint penetration and diameters were then measured using a 10X microscope with a staging compound calibrated in mils.

Figure 17 shows a plot of nugget diameter as a function of welding time. In Fig. 17, the solid and dotted lines represent the model and data, respectively. The finite element model provided reasonable predictions of the weld nugget geometry.

Fig. 15 — Vertical stress distribution; time = 7 cycles

Conclusions

It has been shown that the finite element modeling of the resistance spot welding process can provide good simulation, if the model includes the electro-thermal mechanical interaction and good temperature-dependent material proper-

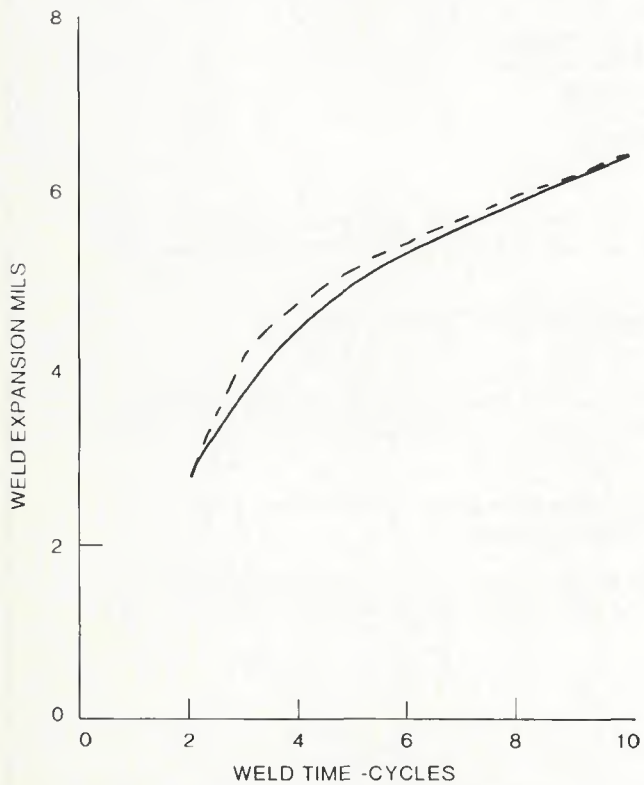

Fig. 16 — Weld nugget expansion vs. weld time; I = 8000 A

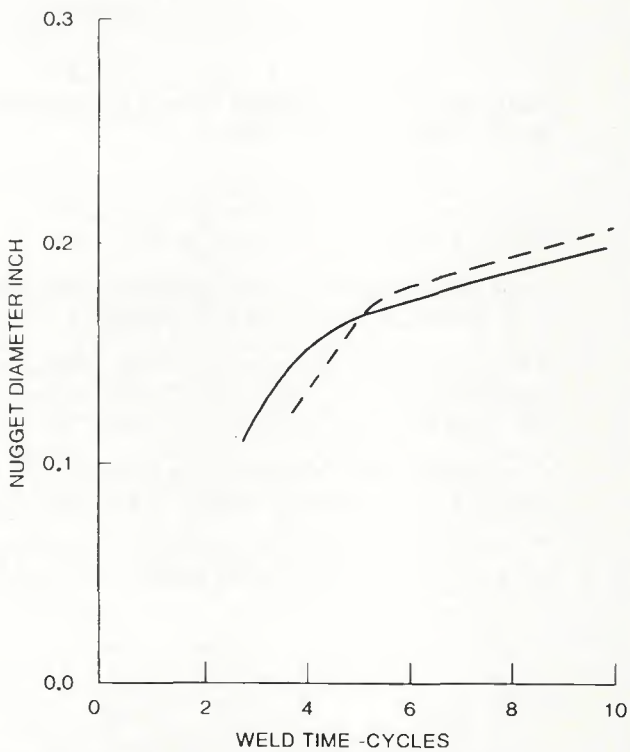

Fig. 17 — Weld nugget diameter vs. weld time; I = 8000 A

ties. It is common practice in industry to use welding conditions tabulated in handbooks as the starting point to develop a welding schedule. The results presented herein indicate that there is another alternative: the use of a realistic analytic model.

Finite element modeling and analysis is a well developed technique. Using this method, one can investigate weld nugget formation for a variety of materials to be joined and different electrode configurations. The use of an analytic tool by the process engineer provides him with another procedure to develop weld schedules before going onto the shop floor to conduct tests.

The finite element model described in this analysis was used as a quantitative framework for developing a multivariable closed-loop control system for the resistance spot welding process (Ref. 12). Many analytic "experiments" were conducted inexpensively using this model to determine the significant variables and the best place to measure them. In addition, the finite element model and the analysis conducted provided a better understanding of the welding physics which would be difficult to determine by experiment alone.

Acknowledgments

The author gratefully acknowledges the support for this project by J. Kelley, E. Helder, and J. Hsai of the General Electric Company, Aircraft Engine Business Group. In addition, the assistance of Mr. Stanley Godwin (Corporate Research and Development) and Mr. John Devine (Gas Turbine Division) in conducting the experiments and tests is gratefully appreciated.

References

1. Bowden, F. P., and Williamson, J. B. P. 1958 (August). Electrical conduction in solids—I. Influence of the passage of current on the contact between solids. *Proc. Royal Soc. of London* 246:1-12.

2. Greenwood, J. A., and Williamson, J. B. P. 1958 (August). Electrical conduction in solids—II. Theory of temperature-dependent conductors. *Proc. Royal Soc. of London* 246:13-31.

3. Greenwood, J. A. 1961. Temperatures in spot welding. *British Welding Journal* 8(6):316-322.

4. Bentley, K. P., Greenwood, J. A., Knowlson, P. McK., and Baker, R. G. 1963. Temperature distributions in spot welds. *BWRA report*, pp. 613-619.

5. Rice, W., and Funk, E. J. 1967. An analytical investigation of the temperature distributions during resistance welding. *Welding Journal* 46(4):175-s to 186-s.

6. Chakalev, A. A. 1973. Evaluation of the thermal state of the metal in spot welding with the help of a computer. *Svar. Proiz.* 10:5-7.

7. Houchens, A. F., Page, R. E., and Young, W. H. 1977. Numerical modeling of resistance spot welding. *Numerical modeling of manufacturing processes*, eds. R. F. Jones, H. Armen, and J. T. Fong, pp. 117-129. ASME WAM, Atlanta, Georgia, Nov. 27-Dec. 2, 1977.

8. Bathe, K.-J., and Wilson, E. L. 1976. *Numerical methods in finite elements*. Prentice-Hall.

9. Erickson, W. C. 1978. *Computer simulation of solidification*. Los Alamos Scientific Laboratory NTIS LA-UR-78-1852.

10. Civelek, M. B., Erdogan, F., and Cakiroglu, A. O. 1978. Interface separation for an elastic layer loaded by a rigid stamp. *Intl. J. Engng. Sci.* 16:669-679.

11. Satoh, T., Katayama, J., and Abe, H. 1969. Temperature distribution and breakdown of oxide layer during resistance spot welding using two-dimensional model. *Annual assy. of I.I.W.—Kyoto: document no. III, 371-69*. Osaka Inst. of Technology, Dept. of Mechanical Engineering.

12. Kuchar, N. R., Cohen, R. K., Nied, H. A., and Godwin, S. J. 1982. A closed loop control system for resistance spot welding. *Measurement and control for batch manufacturing*, ed. D. E. Hardt, pp. 89-103. ASME WAM, Phoenix, Arizona, Nov. 14-19, 1982.

WRC Bulletin 285
July, 1983

Stress Indices and Flexibility Factors for Concentric Reducers
by E. C. Rodabaugh and S. E. Moore

This report was developed as part of the ORNL Piping Program funded by the U. S. Atomic Energy Commission. The recommended stress indices in the report were incorporated into the ASME Boiler and Pressure Vessel Code, Section III, in 1977.

Finite Element Analysis of Eccentric Reducers and Comparisons with Concentric Reducers
by R. R. Avent, M. H. Sadd, and E. C. Rodabaugh

This report was developed to provide stress indices for eccentric reducers, and includes recommendations for relatively minor work changes in the NB-3680 portion of the ASME Code which would extend the coverage to include eccentric reducers.

Publication of these reports was sponsored by the *Sub-Committee on Piping Pumps and Valves* of the *Pressure Vessel Research Committee* of the *Welding Research Council*.

The price of WRC Bulletin 285 is $14.25 per copy plus $5.00 for postage and handling. Orders should be sent with payment to the Welding Research Council, Rm. 1301, 345 E. 47th St., New York, NY 10017.